Journal of Power Sources 195 (2010) 3053–3059

Contents lists available at ScienceDirect

Journal of Power Sources

journal homepage: www.elsevier.com/locate/jpowsour

Characterization of the Ni-ScSZ anode with a LSCM–CeO_2 catalyst layer in thin film solid oxide fuel cell running on ethanol fuel

Bo Huang[a,*], Xin-jian Zhu[a], Wan-qi Hu[b], Yun-yun Wang[a], Qing-chun Yu[a]

[a] Institute of Fuel Cell, Shanghai Jiaotong University, 800 Dongchuan Road, Shanghai 200240, PR China
[b] Institute of Process Engineering, Chinese Academy of Sciences, PR China

ARTICLE INFO

Article history:
Received 26 September 2009
Received in revised form
13 November 2009
Accepted 25 November 2009
Available online 2 December 2009

Keywords:
Electrochemical properties
Carbon deposition
Catalyst layer
Impedance spectroscopy
Solid oxide fuel cell

ABSTRACT

Solid oxide fuel cell (SOFC) running directly on hydrocarbon fuels has attracted much attention in recent years. In this paper, a dual-layer structure anode running on ethanol is fabricated by tape casting and screen-printing method, the addition of a LSCM–CeO_2 catalyst layer to the supported anode surface yields better performance in ethanol fuel. The effect that the synthesis conditions of the catalyst layer have on the performances of the composite anodes is investigated. Single cells with this anode are also fabricated, of which the maximum power density reaches 669 mW cm^{-2} at 850 °C running on ethanol steam. No significant degradation in performance has been observed after 216 h of cell testing when the Ni-ScSZ13 anode is exposed to ethanol steam at 700 °C. Very little carbon is detected on the anode, suggesting that carbon deposition is limited during cell operation. Consequently, the LSCM–CeO_2 catalyst layer on the surface of the supported anode makes it possible to have good stability for long-term operation in ethanol fuel due to low carbon deposition.

1. Introduction

Solid oxide fuel cell (SOFC) is one of the most promising energy conversion devices that convert chemical energy in fossil fuels into electricity. It can be applied not only to alternative thermal power plants but also dispersed power plants and integrated coal gasification combined cycle power plants (IGCC). The state-of-the-art SOFC anode material is the Ni-YSZ cermet [1,2] which offers excellent catalytic properties, mixed conductivity and good current collection. However, such cermets present some disadvantages related to the low tolerance to carbon build up when operating under hydrocarbon fuelling [3,4]. Since Ni is a good catalyst for hydrocarbon cracking reaction. Carbon deposition (coking) covers the active sites of the anode, resulting in rapid, irreversible cell deactivation [5–9]. High steam/carbon ratio is necessary to suppress the carbon deposition, which lowers the electrical efficiency of the system [10].

In order to overcome the disadvantages of Ni-YSZ cermet anode, several alternative materials were investigated as potential anodes in recent years. Ceria-based anodes have important advantages over conventional Ni-based anodes, namely the ability to suppress carbon deposition on electrodes in hydrocarbon (such as methane) atmospheres as the presence of mobile lattice oxygen reduces the rate of carbon deposition [11,12]. However, relatively large lattice expansion associated with the loss of oxygen under anodic conditions can result in the anode spilling off the electrolyte [13]. $LaCrO_3$-based oxide such as $(LaSr)CrO_3$ was also shown to have very low activity towards carbon deposition [14]. Catalytic activity of $LaCrO_3$ for methane oxidation can also be substantially enhanced by partial substitution at A- and B-sites. Sfeir et al. [15] studied the thermodynamic stability and the catalytic activity of $(LaA)(CrB)O_3$ system (A = Ca, Sr and B = Mg, Mn, Fe, Co, Ni) as alternative anode materials under simulated SOFC operation conditions. Thermodynamically, Sr and Mn substitution maintains the stability of the perovskite while other substitutes destabilize the system. Recently, Tao and Irvine [16,17] reported promising results of $La_{0.75}Sr_{0.25}Cr_{0.5}Mn_{0.5}O_3$ (LSCM) as anode for SOFC. LSCM is a p-type conductor with conductivity of ~38 S cm^{-1} in air and 1.5 S cm^{-1} in 5%H_2 at 900 °C. The electrode polarization resistance for the oxidation reactions in wet CH_4 and H_2 at 900 °C was 0.85 and 0.26 Ω cm^2, respectively. The performances are considered to be compatible to the Ni-YSZ cermet anodes. Gorte and his co-workers resolved the problem of carbon deposition by using Cu–CeO_2–YSZ anode [18–21], in which copper acted as current collector while ceria provided a high catalytic activity for hydrocarbon reforming. Due to the low melting point of copper and its oxides, an alternative method in place of traditional high temperature sintering was developed on basis of tape casting and wet-impregnation. The results indicate high electrochemical activity owing to the development of porous structures from very fine particles with a large TPB area. Though the results were encouraging, wet-impregnation

* Corresponding author. Tel.: +86 21 34206249; fax: +86 21 34206249.
E-mail address: huangbo2k@hotmail.com (B. Huang).

0378-7753/$ – see front matter © 2009 Elsevier B.V. All rights reserved.
doi:10.1016/j.jpowsour.2009.11.126

treatment of the porous YSZ material is a time-consuming process. It requires repeated wet-impregnation/sintering treatments for three to five times to obtain a sufficient amount of ionic conductance of the anode structure. Moreover, it is difficult to determine the mass or volume fraction of Cu–CeO_2 impregnated into the porous YSZ material. Most recently, Barnett group reported a new SOFC that combines a Ru–CeO_2 catalyst layer with a conventional anode, allowing internal reforming of iso-octane without coking [22]. However, its use is limited by the high cost of Ru and evaporation above 1200 °C to produce volatile RuO_4 species [23]. $Gd_{0.2}Ce_{0.8}O_2$-coated anodes have shown good performance for the direct utilization of hydrocarbon in SOFC [24].

In this study, a Ni-scandia-stabilized zirconia (ScSZ) cermet anode with a catalyst layer $La_{0.75}Sr_{0.25}Cr_{0.5}Mn_{0.5}O_3$–$CeO_2$ (LSCM–CeO_2) was prepared by screen-printing LSCM–CeO_2 slurry on the surface of Ni-ScSZ anode. This study's focus was to evaluate the impact of a catalyst layer on the catalytic activity and tolerance to carbon deposition of this anode in SOFC fueled by ethanol fuel. The results clearly show that the LSCM–CeO_2 catalyst layer on the surface of Ni-ScSZ anode not only improves the kinetics of hydrogen or ethanol oxidation reaction, but also reduces the degradation in performance of this anode in ethanol fuel.

2. Experimental

2.1. Fabrication of catalyst layer and unit cells

The SOFC devices investigated in this study were typical anode-supported cells. Test cells were generally constructed through a four-layer process which includes: (a) porous LSCM–CeO_2 catalyst layer; (b) porous Ni-ScSZ-supported anode layer (thickness: 0.8 mm); (c) dense ScSZ electrolyte layer; (d) porous PCM ($(Pr_{0.7}Ca_{0.3})_{0.9}MnO_3$) cathode layer. Fig. 1 showed the schematic diagram of anode-supported single cell constructed through a four-layer process.

The material system used in the catalyst layer was based on commercial cerium oxide (CeO_2, Shanghai Chem. Ltd., China) powder and Sr and Mn-doped lanthanum chromites $La_{0.75}Sr_{0.25}Cr_{0.5}Mn_{0.5}O_3$ (LSCM) powder. LSCM material was prepared using a combustion synthesis technique as reported elsewhere [25]. The cell fabrication process is briefed as follows according to the procedure described previously [24]. Commercial nickel oxide (NiO, Inco Canada) powder and scandia-stabilized zirconia $Zr_{0.89}Sc_{0.1}Ce_{0.01}O_{2-x}$ (ScSZ, 99.99% pure, Daiichi Kigenso Kagaku Kogyo, Japan) powder was ball-milled with proper amounts of ammonium oxalate ($(NH_4)_2C_2O_4{\cdot}H_2O$, 200 mesh) as pore former to increase the porosity; azeotropic mixture of butanone and ethyl alcohol absolute as solvent; triethanolamine as a kind of zwitterionic dispersant to reduce the interfacial tension between the surface of the particle and the liquid; polyethylene glycol (PEG 200) as plasticizer to increase the flexibility of the tapes; poly-vinyl-butyl (PVB) as binder to provide their strength after the evaporation of the solvent. Start materials were weighed, mixed and ball-milled, then homogeneous slurry was obtained. The slurry was degassed using a vacuum pump (pressure: 200 mbar absolute) and cast onto glass surface. Anode-supported SOFC was fabricated using a dual tape cast layers of Ni-ScSZ and ScSZ, one containing pore formers (the porous Ni-ScSZ anode matrix) and one without pore formers (the dense ScSZ electrolyte layer). The electrolyte layer was cast first and then allowed to dry at room temperature for 48 h. A second layer of Ni-ScSZ which contained pore formers was then cast on top of the electrolyte green tape and allowed to dry overnight. The composite structure was then co-sintered in the air at 1400 °C for 2 h. Thus a disk-shaped anode-supported composite membrane, having a diameter of about 3.0 cm, a thickness of 0.8 mm, was then produced. The cathode was fabricated by screen-printing a slurry containing PCM onto the surface of the dense ScSZ electrolyte and then sintered at 1200 °C for 3 h. Lastly, the slurry of catalyst layer LSCM–CeO_2 (with weight ratios of 1:0, 1:1 and 1:3) was screen-printed on the anode disks and then sintered at 1100 °C for 3 h. Thus, the Ni-ScSZ anodes with the LSCM–CeO_2 catalyst layer (denoted as Ni-ScSZ10, Ni-ScSZ11 and Ni-ScSZ13, respectively) were obtained. The thickness of the LSCM–CeO_2 catalyst layer was controlled at 8 μm while that of the electrolyte and the cathode was controlled at 15 and 20 μm, respectively, which was demonstrated in field emission scanning electron microscopy (FE-SEM) images using a microscope (FE-SEM, PHILIPS 515, Holland) equipped with an X-ray analyzer for energy-dispersive X-ray spectroscopy (EDS). The cathode surface area was controlled to a known value so that current density can be calculated for electrochemical measurements.

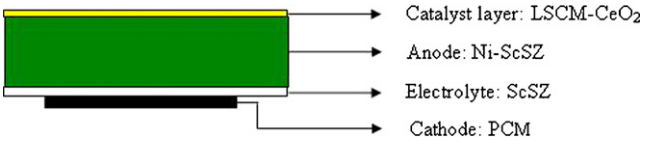

Fig. 1. The schematic diagram of anode-supported single cell constructed through a four-layer process.

2.2. Characterization of single cell performance

Experimental techniques, apparatus and the electrochemical cell assembly for SOFC tests have been described previously [24,25]. A Pt mesh and lead wire were attached to the surface of the cathode using a Pt ink, followed by sintered at 950 °C for 0.5 h. On the anode side, a Au mesh and lead wire were used as the current collector and were attached using a Au ink applied to the edges of the Au mesh, followed by sintering at 850 °C for 0.5 h. The anode side of the structure was then attached to an alumina tube using Au ink and the edges were sealed using a ceramic adhesive. All the anodes were evaluated with the same testing procedure. The anodes were fully reduced in H_2 atmosphere at 850 °C for 2 h prior to cell testing. Hydrogen or gasified ethanol–water mixture (with volume ratio 2:1) were used as fuel and oxygen was used as oxidant. The fuel and oxidant flow rate were all controlled at 25 mL min^{-1}, and the liquid fuel was vaporized by water bath (70 °C) and then brought into the anode surface by nitrogen. The current–voltage curves and electrochemical impedance spectroscopy (EIS) were obtained using an Electrochemical Workstation IM6e (Zahner, GmbH, Germany). These measurements were started after stabilized under a constant discharge voltage of 0.6 V for 4 h in order to obtain a sufficiently stabilized system necessary for a cell testing experiment. Then the current was switched off and the impedance spectra of the electrochemical cell were recorded under open circuit from time to time with amplitude of 20 mV over the frequency range 0.02 Hz to 100 kHz. The measurement was carried out in the temperature range of 700–850 °C in steps of 50 °C. The specific ohmic resistance of the electrolyte, the cathode and the anode ($R\Omega$) was estimated from the high-frequency intercept of the impedance curves and the specific polarization resistance (R_p) was directly measured from the differences between the low and high-frequency intercepts on the impedance curves.

3. Results and discussion

3.1. Performances of single cells

Figs. 2–4 show typical voltage and power density *vs.* current density of the three cells with different catalyst layers while operating on humidified hydrogen (a) and ethanol steam (b), respectively.

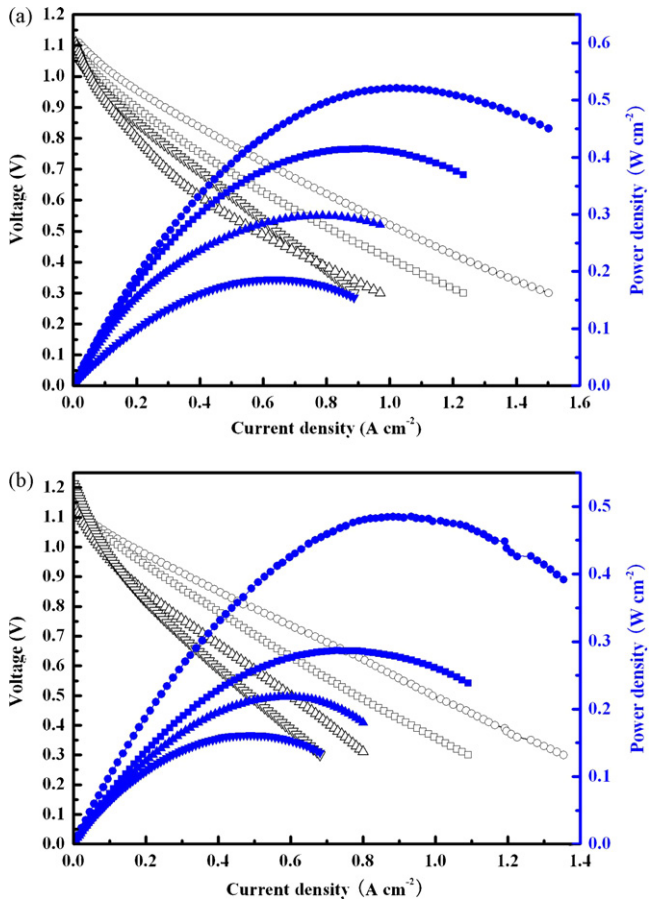

Fig. 2. Voltage and power density *vs.* current density for an SOFC with Ni-ScSZ10 anode while running on humidified hydrogen (a) and ethanol steam (b) at different temperature: (○, ●) 850 °C; (□, ■) 800 °C; (▲, △) 750 °C; (▼, ▽) 700 °C.

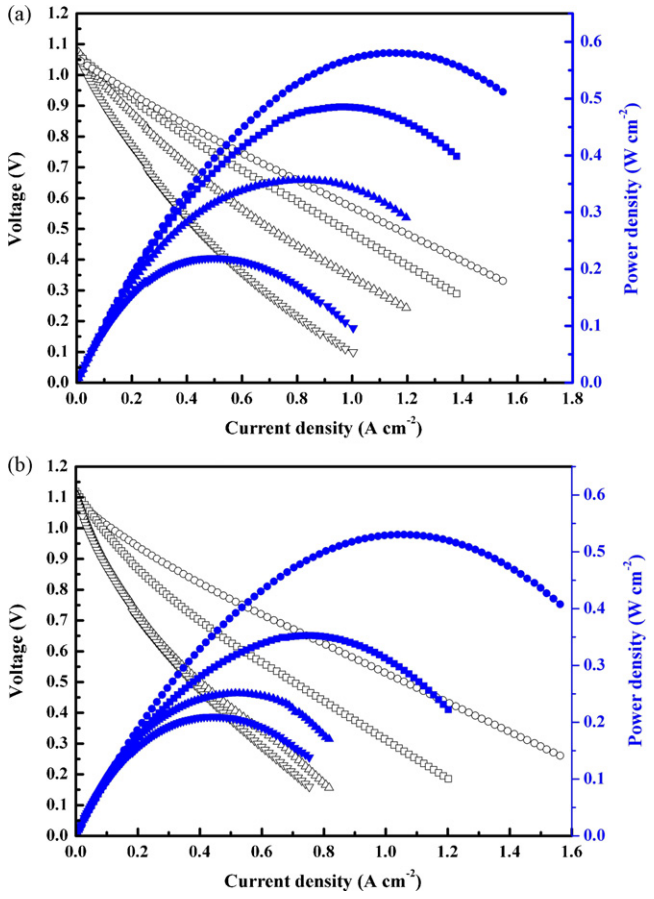

Fig. 3. Voltage and power density *vs.* current density for an SOFC with Ni-ScSZ11 anode while running on humidified hydrogen (a) and ethanol steam (b) at different temperature: (○, ●) 850 °C; (□, ■) 800 °C; (▲, △) 750 °C; (▼, ▽) 700 °C.

The performance of the cell with Ni-ScSZ10 anode while operating on humidified hydrogen was modest with a maximum power density of 521, 413, 298 and 186 mW cm^{-2} at 850, 800, 750 and 700 °C, respectively, and whereas the corresponding values were 586, 485, 356 and 219 mW cm^{-2} for the cell with Ni-ScSZ11 anode, 710, 582, 475 and 354 mW cm^{-2} for the cell with Ni-ScSZ13 anode. The highest power density of the cell with Ni-ScSZ10 anode while operating on ethanol steam was 486, 286, 218 and 161 mW cm^{-2} at 850, 800, 750 and 700 °C, respectively. The counterparts of the cells with Ni-ScSZ11 and Ni-ScSZ13 anodes while operating on ethanol steam was 541, 356, 252 and 206 mW cm^{-2}, 669, 422, 335 and 238 mW cm^{-2}, respectively. Since the electrolyte and cathode were prepared identically, the performance of the three cells depended strongly on the anode composition. The data show an increase in performance of the single cell from cell with Ni-ScSZ10 anode to cell with Ni-ScSZ13 anode while running on humidified hydrogen and ethanol steam. These results indicate the anode performance improves with the increase of CeO_2 content in catalyst layer.

In an attempt to examine the reason for the three cell performances in Figs. 2–4, we measured the impedance spectra of the three cells while running on humidified hydrogen and ethanol steam at 800 °C. Fig. 5 shows a comparison of typical EIS results, from cells with Ni-ScSZ10, Ni-ScSZ11 and Ni-ScSZ13 anodes operating on humidified hydrogen and ethanol steam under open circuit at 800 °C, respectively. The high-frequency intercept of the impedance spectra corresponds to the ohmic resistance of the cell ($R\Omega$), including ohmic resistance of the ScSZ electrolyte, ohmic resistance of the Ni-ScSZ10 (Ni-ScSZ11 or Ni-ScSZ13) anode and the PCM cathode, contact resistance at the electrode/electrolyte interface, and contact resistance between the electrodes and current collector [26]. The high-frequency and low-frequency depressed arcs correspond to different electrochemical processes, typically charge transfer and gas diffusion either or both in the cathode and anode. As above-mentioned, the compositions and preparation conditions for the electrolyte and cathode, as well as the single cell fabrication steps, were identical for the two single cells; therefore, the cathodic polarization resistance and total ohmic resistance of the cells (exclusive of the anode) should be the same. Since the high-frequency arc changed slightly for the different cells, On the other hand, the low-frequency arc changed significantly as the anode composition varied; therefore, it was related to the anodic process taking place on the different anode surface. We could find that total resistance of the single cell increased from cell with Ni-ScSZ13 anode to cell with Ni-ScSZ10 anode while running on humidified hydrogen and ethanol steam. Impedance measurements taken at open circuit voltage for the three cells in humidified hydrogen or ethanol steam presented in Fig. 5 indicated that the LSCM–CeO_2 catalyst layer with much more CeO_2 content caused the polarization resistance to decrease. These results are consistent with the above-mentioned performance of the three cells with different anode catalyst layer.

On one hand, this agrees with previous studies that indicate that CeO_2 promotes hydrocarbon oxidation [27], the high electrocatalytic activity of CeO_2-based materials for hydrocarbon oxidation is most likely due to the extraordinary ability of CeO_2 to store, release and transport oxygen ions [28,29], thus also increasing hydrogen or ethanol oxidation rates in our experiment. On the other hand, we think that in LSCM–CeO_2/Ni-ScSZ anode, LSCM as a p-type con-

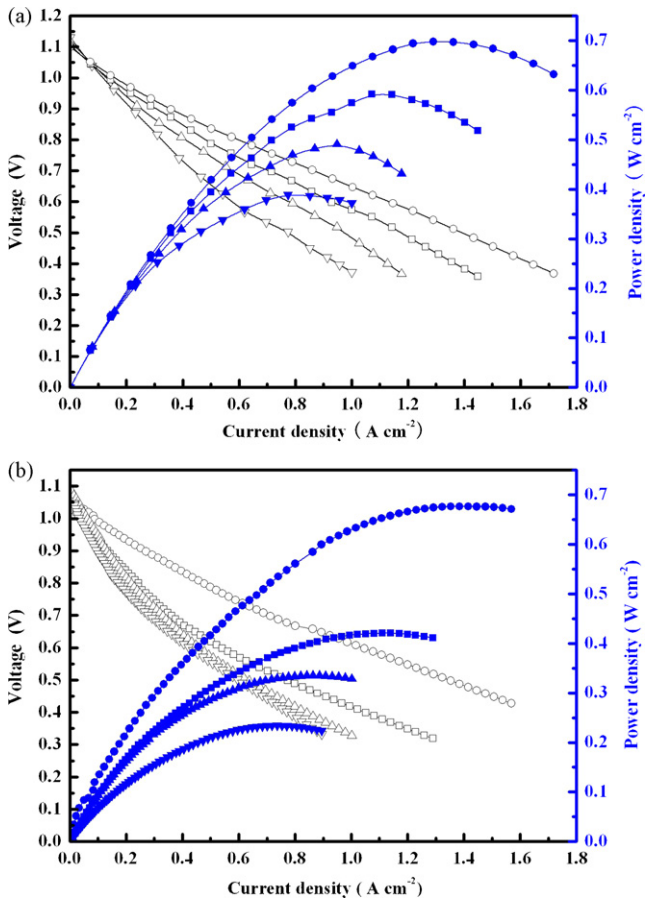

Fig. 4. Voltage and power density *vs.* current density for an SOFC with Ni-ScSZ13 anode while running on humidified hydrogen (a) and ethanol steam (b) at different temperature: (◯, ●) 850 °C; (□, ■) 800 °C; (▲, △) 750 °C; (▼, ▽) 700 °C.

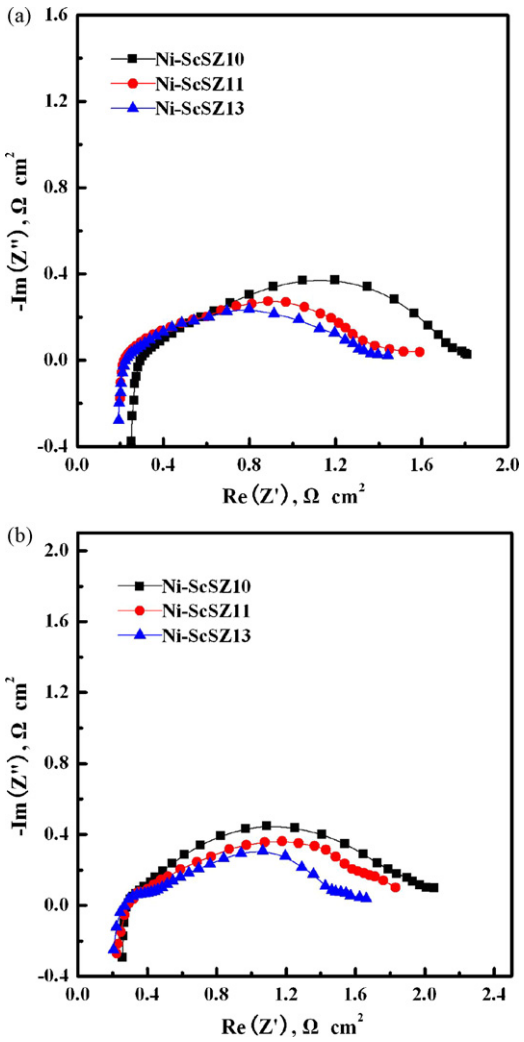

Fig. 5. Electrochemical impedance spectra for an SOFC with different anode while running on humidified hydrogen (a) and ethanol steam (b) at 800 °C under open circuit.

ductor plays important role because it provides the conductivity and connectivity path of the anode system. So when the CeO_2 amount in the anode reaches some value, a certain amount of LSCM will improve the anode performance by providing better conductive network. It is noted that CeO_2 is a good promoter for Ni in reforming catalysis. In the dual-layer anode structure, by having the LSCM–CeO_2 catalyst layer at the top of the supported anode in contact with Ni, the case is probably that ethanol steam reforming takes place in the catalyst layer first, and then the supported anode catalyses the oxidation of the products of internal reforming and provides the conductivity of the whole anode, which means that the catalysis of ethanol on CeO_2 is much more important in the dual-layer anode structure. Therefore, we deduce that CeO_2 can reform the ethanol before it can get to the Ni part of the supported anode.

As we know, the two reactions (1) and (2) mainly occur when ethanol steam are fed to the catalyst layer, since Ni is much active a catalyst for hydrogen oxidation than for carbon monoxide oxidation, performance in hydrogen is better than that in ethanol. Probably when CeO_2 content in the catalyst layer increased, the catalyst is much effective for hydrogen production with high selectivity for reaction (2), and the water gas shift of (3) is also a possible reaction to generate hydrogen. The impedance spectra in Fig. 5 also demonstrated that the cell with Ni-ScSZ13 anode had much smaller polarization resistance than the cells with Ni-ScSZ10 and Ni-ScSZ11 anodes possibly because of much more hydrogen production and its quicker diffusion:

$$C_2H_5OH + H_2O \rightarrow 2CO + 4H_2 \quad (1)$$

$$C_2H_5OH + 3H_2O \rightarrow 2CO_2 + 6H_2 \quad (2)$$

$$CO + H_2O \rightarrow CO_2 + H_2 \quad (3)$$

Attending to the microstructure, Fig. 6 shows the FE-SEM micrograph of the interface LSCM–CeO_2/Ni-ScSZ after fuel cell test in ethanol steam at 700 °C for 200 h (Ni-ScSZ10 (a)) and 216 h (Ni-ScSZ13 (b)), respectively. The figure also shows the FE-SEM micrograph of the LSCM–CeO_2 catalyst layer (about 8 μm). The microstructure of the LSCM–CeO_2 catalyst layer is very promising, a porous structure made of sintered LSCM and CeO_2 particles. The SEM images of the interface LSCM–CeO_2/Ni-ScSZ in Fig. 6 show that the LSCM–CeO_2 catalyst layer is well adhered to the Ni-ScSZ-supported anode layer even after 200 and 216 h operation in ethanol steam.

3.2. Cell stability tests

Carbon deposition on steam reforming catalysts is a problem known to petrochemical industry for a long time, especially in the presence of nickel catalyst [30]. We used LSCM in the catalyst layer, which is inert for carbon formation, however, considering Ni in the Ni-ScSZ-supported anode layer, the long-term stability of the two-layer structure anode should be studied to make sure whether coking occurs while running on ethanol steam for a long time.

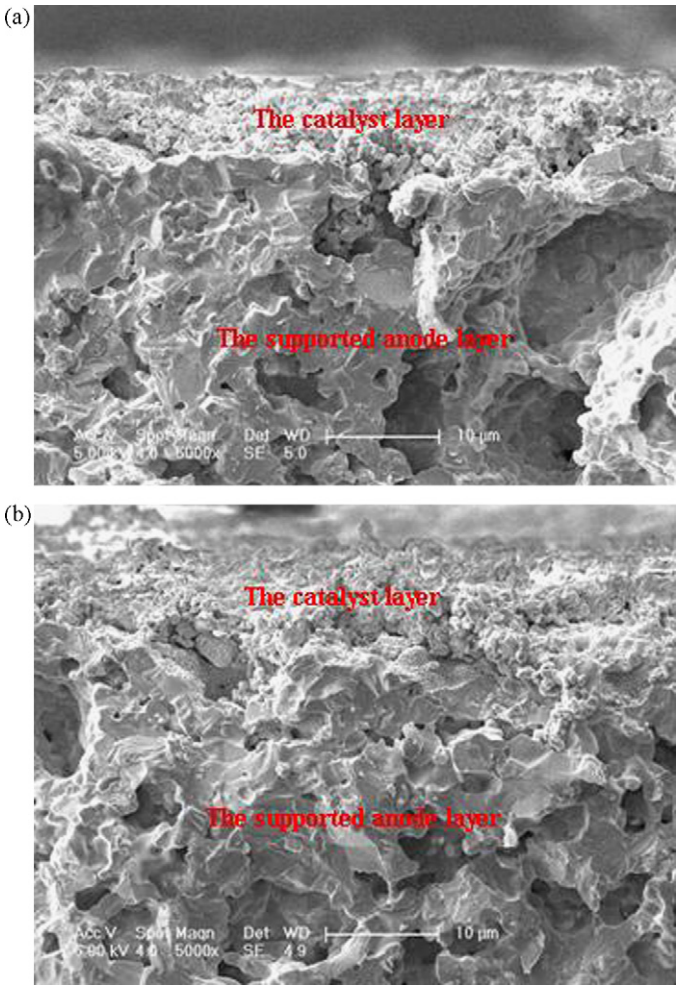

Fig. 6. FE-SEM micrograph of the interface LSCM–CeO_2/Ni-ScSZ after fuel cell test in ethanol steam at 700 °C for 200 h (Ni-ScSZ10 (a)) and 216 h (Ni-ScSZ13 (b)), respectively.

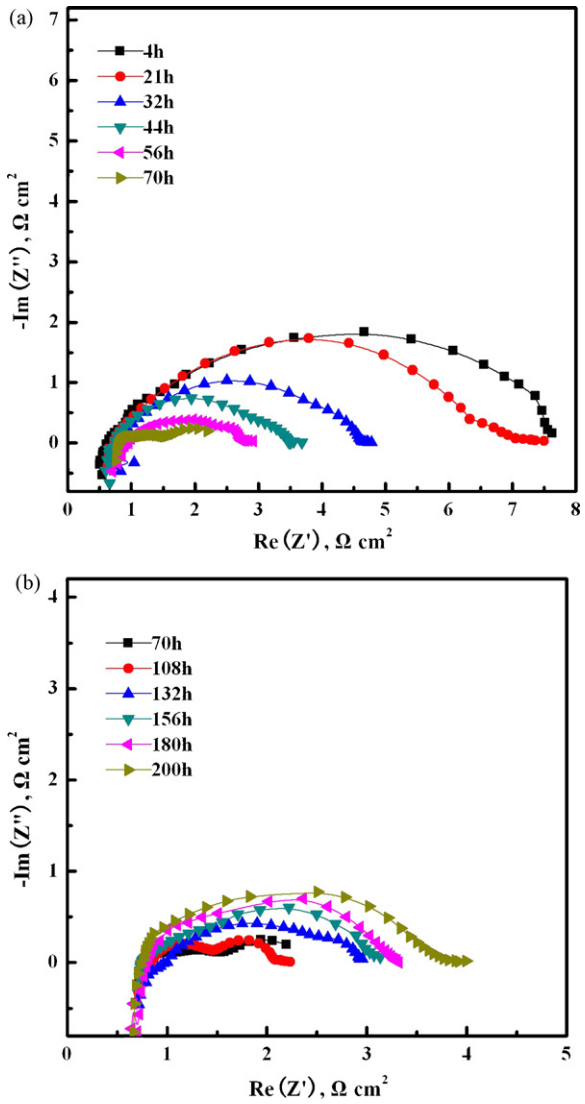

Fig. 7. Electrochemical impedance spectra of Ni-ScSZ10 anode in ethanol steam at 700 °C under open circuit during the aging process.

The stabilization and the degradation of the two cells with Ni-ScSZ10 and Ni-ScSZ13 anodes were also investigated in ethanol steam at 700 °C during the measurements. The electrochemical impedance spectra were measured during the aging process. Figs. 7 and 8 depict the electrochemical impedance spectra at 700 °C under open circuit at different operating time for the two cells with Ni-ScSZ10 and Ni-ScSZ13 anodes, respectively. As can be seen from Figs. 7 and 8, the polarization resistance (R_p) is decreasing with time. This implies that, in the case of two anode materials, the electrochemical reaction rates are increasing with time. Then, R_p increases gradually with time suggesting that the corresponding electrochemical reaction rates are decreasing slowly with time (in terms of Ni-ScSZ10 and Ni-ScSZ13, after 70 and 102 h, respectively). The variation of the polarization resistance with time for the two cells with Ni-ScSZ10 and Ni-ScSZ13 anodes indicates that the electrochemical oxidation reaction of ethanol steam are not taking place under constant conditions, rather the conditions at the anode surface are modified with the time of exposure to ethanol steam. These surface modifications affect electrochemical performance of anode samples. However, some of the ethanol steam will make its way to the Ni-ScSZ-supported anode layer during operation considering the thickness of the LSCM–CeO_2 catalyst layer. Therefore, the changes in the impedance spectra can eventually be assumed to be due to carbon deposition in the Ni-ScSZ-supported anode layer, which happened after operation of 21 and 46 h in terms of Ni-ScSZ10 and Ni-ScSZ13 anode, respectively. Visual inspection of the cell after the end of the test revealed very little carbon deposition in the anode layer (Fig. 6). The decrease of the R_p after carbon deposition can be understood by the model similar to that proposed by Gorte and co-workers [31]. Metal Ni in the anode acts also for the efficient current collection. Some metal Ni particles are expected to be not connected to the outside circuit and cannot assist in the removal of electrons. Therefore, the entire region under the isolated metal Ni particle is ineffective for the electrochemical reaction. With the addition of moderate levels of carbon, these isolate metal Ni particles could become electronically connected to the outside circuit. Because more of the anode surface is now involved in the electrochemical reaction, the effect of using a higher fraction of the surface will be an apparent decrease in polarization resistances. With the addition of a certain levels of carbon, deposited carbon began to cover the active sites of the anode and block the pores of gas diffusion, resulting in an increase in polarization resistances. As above-mentioned, CeO_2 can reform the ethanol before it can get to the Ni part of the supported anode, the cell with Ni-ScSZ13 anode had much smaller polarization resistance than the cells with Ni-ScSZ10 and Ni-ScSZ11 anodes possibly because of much more hydrogen production and its quicker diffusion. Therefore, we think the LSCM–CeO_2 catalyst layer retarded the occurrence of carbon

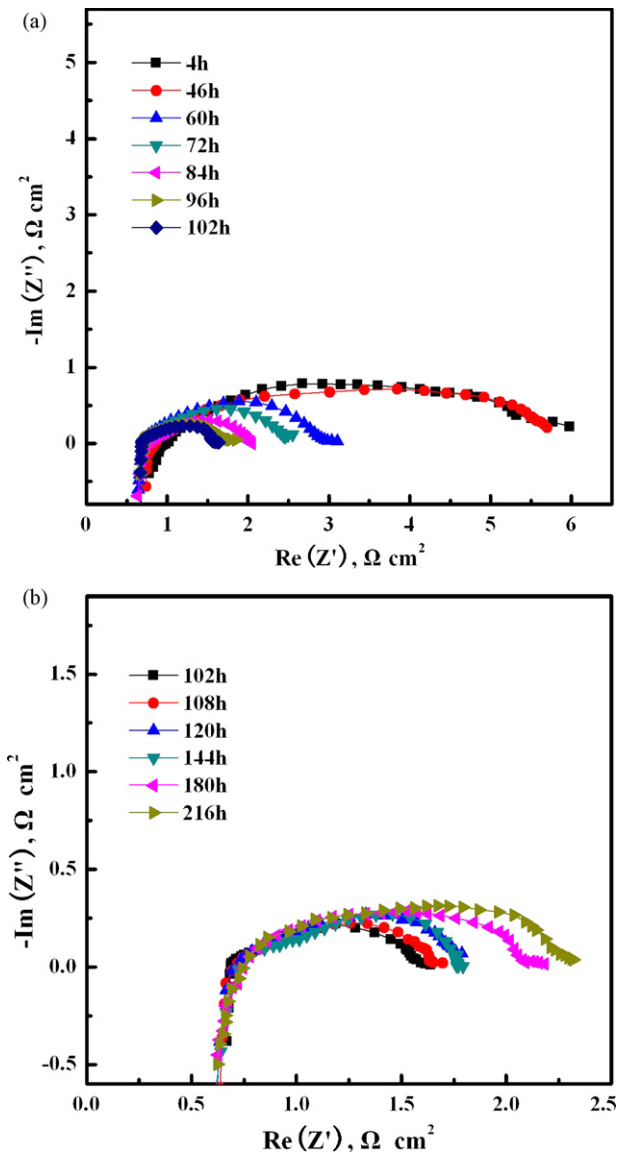

Fig. 8. Electrochemical impedance spectra of Ni-ScSZ13 anode in ethanol steam at 700 °C under open circuit during the aging process.

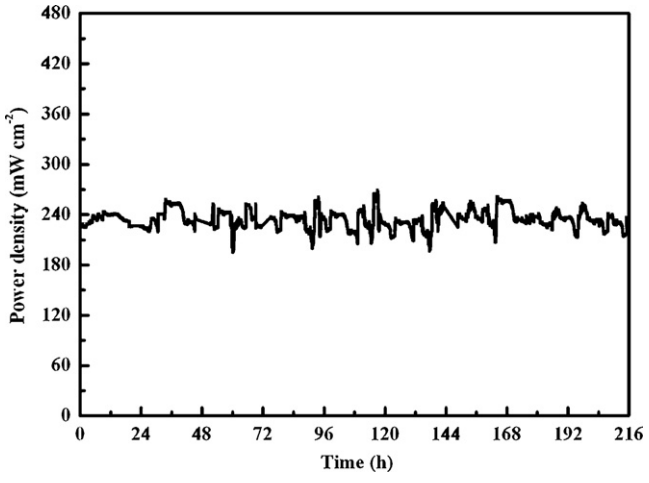

Fig. 9. Power density at 0.6 V for an SOFC with Ni-ScSZ13 anode using ethanol steam as fuel and oxygen as oxidant at 700 °C during the aging process.

deposition of the Ni-ScSZ-supported anode, especially when CeO_2 content in the catalyst layer increased.

The stabilization and degradation of the cell with Ni-ScSZ13 anode were also investigated in ethanol steam at 700 °C during the measurements. We recorded the curve of power density for the cell operating on ethanol steam as a function of time by discharging at 0.6 V at 700 °C, shown in Fig. 9. We can find that the performance of the cell almost kept constant with a little augment of power density with time in the period of 216 h. In one case, the cell was operated for >216 h in ethanol steam at 700 °C, before the test was stopped with the cell still running well. Almost no carbon deposits were detected after testing in ethanol steam at 700 °C for >216 h on the Ni-ScSZ13 anode under conditions in the present study, suggesting that carbon deposition was limited during cell operation.

4. Conclusions

A dual-layer structure anode running on ethanol steam was fabricated by tape casting and screen-printing method in this paper, and the addition of a LSCM–CeO_2 catalyst layer to the support anode surface yielded much better performance in ethanol steam probably due to the ethanol steam reforming reaction takes place in the catalyst layer. CeO_2 plays much important role in the catalyst layer. The anode performance improves with the increase of CeO_2 content in catalyst layer, for example, the single cell with LSCM–CeO_2 (with weight ratio 1:3) catalyst layer calcined at 1100 °C shows both good performance with the maximum power density reached 669 mW cm^{-2} at 850 °C and long-term stability in ethanol steam for 216 h with little carbon formation. Fabrication of this structure for long-term stability continues to be a potential concern, and the conversion over ethanol feed needs determining to improve internal reforming efficiency by analyzing the exit gas later. Further studies should be concerned with the composition and microstructure in both the catalyst layer and the supported anode layer to enhance the anode performance.

Acknowledgement

The authors thank the National “863” Program of China (No. 2007AA05Z138) for the grants that support this research.

References

[1] S.P. Jiang, S.H. Chan, Mater. Sci. Technol. 20 (2004) 1109.
[2] S.P. Jiang, S.H. Chan, J. Mater. Sci. 39 (2004) 4405.
[3] Y. Matsuzaki, I. Yasuda, Solid State Ionics 132 (2000) 261.
[4] B.C.H. Steele, I. Kelly, H. Middleton, R. Rudkin, Solid State Ionics 28 (1988) 1547.
[5] C.H. Bartholomew, Catal. Rev. Sci. Eng. 24 (1982) 67.
[6] R.T.K. Baker, Carbon 27 (1989) 315.
[7] B.C.H. Steele, Solid State Ionics 86–88 (1996) 1223.
[8] K. Hernadi, A. Fonseca, J.B. Nagy, A. Siska, I. Kiricsi, Appl. Catal. A 199 (2000) 245.
[9] J.H. Koh, Y.-S. Yoo, J.-W. Park, H.C. Lim, Solid State Ionics 149 (2002) 157.
[10] K. Sasaki, Y. Teraoka, J. Electrochem. Soc. 150 (2003) A878.
[11] I.S. Metcalfe, Solid State Ionics 57 (1992) 259.
[12] V.D. Belyaev, T.I. Politova, O.A. Marina, V.A. Sobyanin, Appl. Catal. A.: Gen. 133 (1995) 47.
[13] M. Mogensen, T. Lindegaard, U.R. Hansen, G. Mogensen, J. Electrochem. Soc. 141 (1994) 2122.
[14] J. Vulliet, B. Morel, J. Laurencin, G. Gauthier, L. Bianchi, S. Giraud, J.Y. Henry, F. Lefebvre-Joud, S.C. Singhal, M. Dokiya (Eds.), SOFC-VIII, vol. 2003–07, The Electrochem. Soc., Pennington, NJ, 2003, p. 803.
[15] J. Sfeir, J. Power Sources 118 (2003) 276.
[16] S. Tao, J.T.S. Irvine, Nat. Mater. 2 (2003) 320.
[17] S. Tao, J.T.S. Irvine, J. Electrochem. Soc. 151 (2004) A252.
[18] S. Park, J.M. Vohs, R.J. Gorte, Nature (London) 404 (2000) 265.
[19] R.J. Gorte, S. Park, J.M. Vohs, C. Wang, Adv. Mater. 12 (2000) 1465.
[20] S. McIntosh, R.J. Gorte, Chem. Rev. 104 (2004) 4845–4865.
[21] T. Kim, G. Liu, M. Boaro, S.-I. Lee, J.M. Vohs, R.J. Gorte, O.H. Al-Madhi, B.O. Dabbousi, J. Power Sources 155 (2006) 231–238.
[22] Z. Zhan, S.A. Barnett, Solid State Ionics 176 (2005) 871–879.

[23] S.P. Jiang, S.H. Chan, J. Mater. Sci. 39 (2004) 4405–4439.
[24] B. Huang, X.F. Ye, S.R. Wang, X.F. Sun, H.W. Nie, J. Shi, Q. Hu, T.L. Wen, J. Power Sources 162 (2006) 1172.
[25] B. Huang, S.R. Wang, R.Z. Liu, X.F. Ye, H.W. Nie, X.F. Sun, T.L. Wen, J. Power Sources 167 (2007) 39.
[26] Y. Leng, S. Chan, K. Khor, S. Jiang, Int. Hydrogen Energy 29 (2004) 1025.
[27] B.C.H. Steele, P.H. Middleton, R.A. Rudkin, Solid State Ionics 40–41 (1990) 388.
[28] N.V. Skorodumova, S.I. Simak, B.I. Simak, B.I. Lundqvist, I.A. Abrikosov, B. Johansson, Phys. Rev. Lett. 89 (2002) 166601.
[29] C.E. Hori, H. Permana, K.Y. Simon Ng, A. Brenner, K. More, K.M. Rahmoeller, D. Belton, Appl. Catal. B 16 (1998) 105.
[30] J. Macek, B. Novosel, M. Marinsek, J. Eur. Ceram. Soc. 27 (2007) 487–491.
[31] H. Kim, C. Lu, W.L. Worrell, J.M. Vohs, R.J. Gorte, J. Electrochem. Soc. 149 (3) (2002) A247.